Science Get Journal
Vol. 03 , No. 2 , April 2026, 19-32
e-ISSN: 3062-6595

Zeolite Nanocomposites from Coal Fly Ash for Arsenic Removal in Wastewater

Erlinda Ningsih[1]*, Hanifah Sriamelia[2], & Salsabilla[3]
[1*]Institut Teknologi Adhi Tama Surabaya, Indonesia, [2]Universitas Negeri Padang, Indonesia,
[3]Universitas Negeri Padang, Indonesia
*Co e-mail: erlindaningsih84@itats.ac.id[1]

Article Information
Received: March 31, 2026
Revised: May 01, 2026
Online: May 08, 2026

Keywords
Coal Fly Ash, Zeolite, Nanocomposite, Arsenic, Adsorption, Wastewater Treatment

ABSTRACT

Arsenic contamination in wastewater poses serious environmental and public health risks because of its toxicity, persistence, and bioaccumulation potential. This study investigated the synthesis and performance of magnetic zeolite nanocomposites (MZN) derived from coal fly ash (CFA) for efficient As(V) removal from wastewater. CFA obtained from the PT PLN Ombilin Power Plant, West Sumatra, Indonesia, was converted into zeolite NaA/NaX through an alkaline hydrothermal method and subsequently modified with Fe_3O_4 nanoparticles to enhance adsorption capacity and magnetic separability. The synthesized MZN was characterized using X-ray diffraction (XRD), Fourier transform infrared spectroscopy (FTIR), scanning electron microscopy with energy dispersive X-ray analysis (SEM-EDX), Brunauer–Emmett–Teller (BET), and vibrating sample magnetometer (VSM) analyses. Batch adsorption experiments were conducted to evaluate the effects of pH, contact time, adsorbent dosage, initial arsenic concentration, and temperature on adsorption performance. The maximum As(V) removal efficiency reached 97.4% under optimum conditions of pH 6, adsorbent dosage of 2 g/L, and contact time of 120 min. Adsorption behavior followed the Langmuir isotherm and pseudo-second-order kinetic models, indicating monolayer chemisorption. Thermodynamic analysis confirmed a spontaneous and endothermic process. Regeneration tests showed that MZN maintained over 85% removal efficiency after five adsorption–desorption cycles, demonstrating its potential as an effective, reusable, and low-cost adsorbent for industrial wastewater treatment.

Keywords: *Coal Fly Ash, Zeolite, Nanocomposite, Arsenic, Adsorption, Wastewater Treatment*

http://doi.org/10.69855/science.v3i2.575
https://gpijournal.com/index.php/science
PUBLISHED BY : GPress Indonesia

INTRODUCTION

Arsenic (As) is a toxic metalloid widely recognized as a major environmental pollutant and a serious threat to human health. The International Agency for Research on Cancer classifies inorganic arsenic compounds as Group 1 human carcinogens due to their strong association with skin, lung, bladder, kidney, and liver cancers. Chronic exposure to arsenic-contaminated water can also cause cardiovascular disease, diabetes mellitus, neurological disorders, and skin lesions (WHO, 2022; Naujokas et al., 2013). Because of these severe health impacts, the World Health Organization established a maximum arsenic concentration of 10 μg/L in drinking water, while Indonesian environmental regulations limit arsenic concentrations in industrial wastewater discharge to 50 μg/L.

Arsenic contamination in aquatic environments originates from both natural and anthropogenic activities. Natural sources include volcanic activity, mineral weathering, and geochemical dissolution of arsenic-bearing rocks, whereas anthropogenic sources mainly arise from mining activities, coal combustion, metal smelting, and excessive application of arsenic-containing pesticides and fertilizers (Smedley & Kinniburgh, 2002). In Indonesia, coal-fired power plants and artisanal gold mining operations are among the dominant contributors to arsenic pollution. Previous studies reported elevated arsenic concentrations in groundwater and river systems surrounding mining and industrial areas in Sumatra, Sulawesi, and Kalimantan, indicating significant risks to environmental quality and public health (Marselina et al., 2020; Irfan et al., 2021).

Numerous technologies have been developed for arsenic removal from wastewater, including coagulation-flocculation, ion exchange, membrane filtration, electrocoagulation, and reverse osmosis. Among these methods, adsorption has attracted considerable attention because of its operational simplicity, relatively low cost, high removal efficiency, and feasibility for adsorbent regeneration (Mohan & Pittman, 2007; Kumar et al., 2019). Nevertheless, many commercial adsorbents suffer from limitations such as high production costs, low selectivity, poor regeneration performance, and secondary sludge generation. Therefore, the development of sustainable and low-cost adsorbent materials remains an important research priority.

Coal fly ash (CFA), a solid waste generated from coal combustion in thermal power plants, has gained increasing attention as a potential raw material for adsorbent synthesis. Indonesia produces millions of tons of CFA annually, yet a substantial proportion remains underutilized and is disposed of in landfills, potentially causing environmental problems (Yao et al., 2015). CFA contains high amounts of silica (SiO_2) and alumina (Al_2O_3), which are suitable precursors for zeolite synthesis through alkaline hydrothermal treatment. Zeolites synthesized from CFA possess high surface area, porous crystalline structures, and abundant active sites that enhance adsorption performance toward heavy metals and metalloids (Querol et al., 2002).

Recent studies have demonstrated that modification of zeolites with iron oxide nanoparticles significantly improves arsenic adsorption efficiency. Iron oxide materials exhibit strong affinity toward arsenate species through ligand exchange and inner-sphere complexation mechanisms (Zhang et al., 2020). Furthermore, incorporation of Fe_3O_4 nanoparticles provides magnetic properties that facilitate rapid adsorbent separation and recovery after treatment, thereby improving

operational practicality and reducing processing costs. Although several studies have investigated fly ash-derived zeolites or iron-based adsorbents independently, integrated development of magnetic zeolite nanocomposites derived from Indonesian CFA for arsenic remediation remains scarcely explored.

The novelty of this study lies in the integration of coal fly ash valorization, hydrothermal zeolite synthesis, and Fe_3O_4 nanoparticle modification to produce a recyclable magnetic zeolite nanocomposite specifically designed for arsenic removal from wastewater. Unlike previous studies that mainly focused on conventional zeolite synthesis or non-magnetic adsorbents, this research comprehensively evaluates the physicochemical characteristics, adsorption behavior, kinetics, thermodynamics, and regeneration performance of the synthesized material using CFA obtained from the Ombilin coal-fired power plant in West Sumatra, Indonesia. This approach not only contributes to sustainable waste utilization and circular economy implementation but also offers a cost-effective and environmentally friendly adsorbent for arsenic-contaminated wastewater treatment.

METHODS

The methodology employed in this study consisted of material preparation, synthesis of magnetic zeolite nanocomposites, characterization analyses, and batch adsorption experiments to evaluate the effectiveness of arsenic removal from wastewater. The detailed procedures and materials used are described as follows.

1. Materials

Coal fly ash (CFA) was collected from the electrostatic precipitator unit of the PT PLN (Persero) Ombilin Steam Power Plant, Sawahlunto, West Sumatra, Indonesia. The collected CFA was stored in sealed polyethylene containers prior to use. Sodium hydroxide (NaOH, ≥99%), sodium aluminate ($NaAlO_2$), ferrous sulfate heptahydrate ($FeSO_47H_2O$), ferric chloride hexahydrate ($FeCl_3{\cdot}6H_2O$), ammonium hydroxide (NH_4OH, 25%), and sodium arsenate dibasic heptahydrate ($Na_2HAsO_4{\cdot}7H_2O$) were purchased from Sigma-Aldrich and Merck. All chemicals were analytical grade and used without further purification. Deionized water (18.2 MΩ·cm) was supplied using a Millipore Milli-Q ultrapure water purification system (MilliporeSigma, USA) throughout all synthesis and adsorption experiments.

2. Characterization of Coal Fly Ash

The particle size distribution of CFA was analyzed using laser diffraction (Malvern Mastersizer 3000). Chemical composition was determined by X-ray fluorescence (XRF, Shimadzu EDX-7000), while mineralogical phases were identified using X-ray diffraction (XRD, PANalytical X'Pert PRO, Cu Kα radiation, λ = 1.5406 Å, scanning range 2θ = 5–80°). Loss on ignition (LOI) was measured by calcination at 750°C for 2 h according to ASTM C618 standards. The chemical composition of Ombilin CFA is presented in Table 1.

Table 1. Chemical composition of Ombilin coal fly ash

No.	Chemical Formula	Content (wt%)
1	SiO_2	58.42
2	Al_2O_3	22.17
3	Fe_2O_3	7.83
4	CaO	3.54
5	MgO	1.22
6	TiO_2	1.05
7	Na_2O	0.89
8	LOI	3.15

The results in Table 1 indicate that SiO_2 and Al_2O_3 were the dominant constituents, confirming that the CFA was suitable as a precursor for zeolite synthesis due to its high aluminosilicate content (Querol et al., 2002; Yao et al., 2015).

3. Zeolite Synthesis from Coal Fly Ash

Zeolite NaX was synthesized using the alkaline fusion-hydrothermal method adapted from Querol et al. (2002). Briefly, 50 g of CFA was mixed with NaOH at a mass ratio of 1:1.2 and fused at 550°C for 1 h in a muffle furnace. The fused product was dissolved in 250 mL deionized water at 80°C for 2 h under continuous stirring. The resulting aluminosilicate solution was aged at room temperature for 24 h before hydrothermal crystallization in Teflon-lined autoclaves at 100°C for 12 h. The synthesized zeolite was filtered, washed to neutral pH, and dried at 80°C for 12 h. The Si/Al molar ratio was maintained at 1.25 to favor NaX framework formation.

4. Synthesis of Magnetic Zeolite Nanocomposites (MZN)

Magnetic zeolite nanocomposites (MZN) were synthesized through co-precipitation of Fe_3O_4 nanoparticles onto zeolite NaX surfaces following the method reported by Zhang et al. (2020) with slight modifications. Five grams of synthesized zeolite were dispersed in 200 mL deionized water using ultrasonication for 30 min. Subsequently, $FeSO_4{\cdot}7H_2O$ (0.01 mol) and $FeCl_3{\cdot}6H_2O$ (0.02 mol) were added under nitrogen atmosphere. NH_4OH solution (25%) was introduced dropwise until pH 10–11 was achieved at 60°C under mechanical stirring (400 rpm) for 60 min. The resulting black precipitate was magnetically separated, repeatedly washed with deionized water, and vacuum-dried at 60°C for 24 h. Preliminary optimization experiments showed that 20 wt% Fe_3O_4 loading produced the highest arsenic adsorption performance.

5. Characterization of MZN

The synthesized MZN was characterized using XRD, FTIR (PerkinElmer Spectrum 100, 4000–400 cm^{-1}), SEM-EDX (JEOL JSM-6510LA), BET surface area analysis (Micromeritics ASAP 2020), and vibrating sample magnetometry (VSM, Lakeshore 7404). BET textural properties of CFA, zeolite NaX, and MZN are summarized in Table 2.

Table 2. BET textural properties of CFA, zeolite NaX, and MZN

Sample	SBET (m^2/g)	Vp (cm^3/g)	Dp (nm)
Coal Fly Ash	1.8	0.004	8.2
Zeolite NaX	412.6	0.218	2.1
MZN	287.3	0.195	2.7

SBET = BET surface area; Vp = total pore volume; Dp = average pore diameter.

As shown in Table 2, zeolite synthesis significantly increased the surface area compared to raw CFA, while Fe_3O_4 incorporation slightly reduced SBET due to partial pore coverage by iron oxide nanoparticles.

6. Batch Adsorption Experiments

A 1000 mg/L As(V) stock solution was prepared by dissolving $Na_2HAsO_4{\cdot}7H_2O$ in deionized water, followed by serial dilution to obtain working solutions. Batch adsorption experiments were conducted in 250 mL Erlenmeyer flasks agitated at 150 rpm. Unless otherwise specified, experiments were performed at pH 6.0, initial arsenic concentration of 10 mg/L, adsorbent dosage of 2 g/L, and temperature of 25 ± 1°C.

The effects of pH (3–10), contact time (0–180 min), initial arsenic concentration (1–50 mg/L), adsorbent dose (0.5–4 g/L), and temperature (25–55°C) were systematically evaluated. Residual arsenic concentrations were analyzed using graphite furnace atomic absorption spectroscopy (Perkin-Elmer AAS 400; detection limit 0.05 µg/L).

The removal efficiency and adsorption capacity were calculated using Equations (1) and (2):

$$RE(\%) = C0(C0 - Ce) \times 100 \qquad (1)$$

$$q_t = \frac{(C_0 - C_t)V}{m} \qquad (2)$$

where C_0(mg/L) is the initial arsenic concentration, C_e(mg/L) is the equilibrium concentration, C_t(mg/L) is the concentration at time t, V(L) is the solution volume, and m(g) is the adsorbent mass.

RESULTS

The results obtained from characterization analyses and adsorption experiments provide important information regarding the structural properties, adsorption behavior, and arsenic removal performance of the synthesized magnetic zeolite nanocomposites. The detailed findings are presented as follows.

1. Characterization of Materials

XRD analysis confirmed the successful transformation of CFA into zeolite NaX with characteristic diffraction peaks at 2θ = 6.3°, 10.1°, 11.9°, 15.6°, 18.7°, 20.3°, and 23.6°, corresponding

to the faujasite (FAU) structure (JCPDS No. 38-0236). After Fe_3O_4 incorporation, additional diffraction peaks appeared at 2θ = 30.2°, 35.5°, 43.1°, 57.0°, and 62.8° (JCPDS No. 19-0629), confirming the presence of magnetite nanoparticles in the magnetic zeolite nanocomposite (MZN). Importantly, the primary zeolite diffraction peaks remained unchanged after Fe_3O_4 loading, indicating that the zeolite framework retained its structural integrity during co-precipitation. The crystallinity index of MZN slightly decreased from 84.7% to 79.2%, suggesting minor pore coverage by Fe_3O_4 nanoparticles without collapse of the FAU framework. This structural stability is essential for maintaining adsorption capacity and reusability.

FTIR spectra further confirmed the successful synthesis of MZN. As shown in Figure 1, characteristic zeolite bands were observed at 1045 cm^{-1} (asymmetric T–O stretching), 786 cm^{-1} (symmetric T–O stretching), 568 cm^{-1} (double-ring vibration), and 459 cm^{-1} (T–O–T bending). After Fe_3O_4 modification, the Fe–O vibration band appeared at 583 cm^{-1}, confirming magnetite incorporation. In addition, the broad O–H stretching band around 3435 cm^{-1} became more intense after adsorption, indicating the involvement of hydroxyl groups in arsenic binding through ligand exchange and surface complexation. A slight shift of the Fe–O and O–H bands after adsorption provided direct experimental evidence of interaction between arsenate species and Fe–OH active sites.

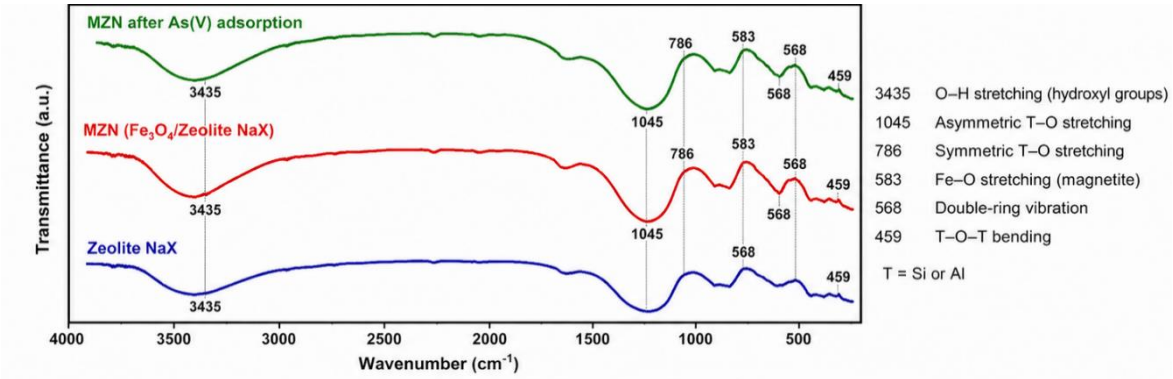

Figure 1. FTIR Spectra of Zeolite NaX, MZN, and MZN after As(V) Adsorption

SEM images (Figure 2) showed that raw CFA mainly consisted of smooth spherical particles with an average diameter of 18.4 μm, while synthesized zeolite NaX exhibited cubic-octahedral crystals ranging from 2–8 μm. Following Fe_3O_4 incorporation, nanosized particles were uniformly distributed on the zeolite surface, resulting in increased surface roughness and pore heterogeneity. Quantitative particle size analysis based on ImageJ evaluation of SEM micrographs showed Fe_3O_4 nanoparticles with an average diameter of 12.8 ± 3.2 nm, consistent with crystallite size estimated using the Scherrer equation. The particle size distribution histogram confirmed homogeneous dispersion of Fe_3O_4 on the zeolite surface, minimizing nanoparticle agglomeration and maximizing active adsorption sites.

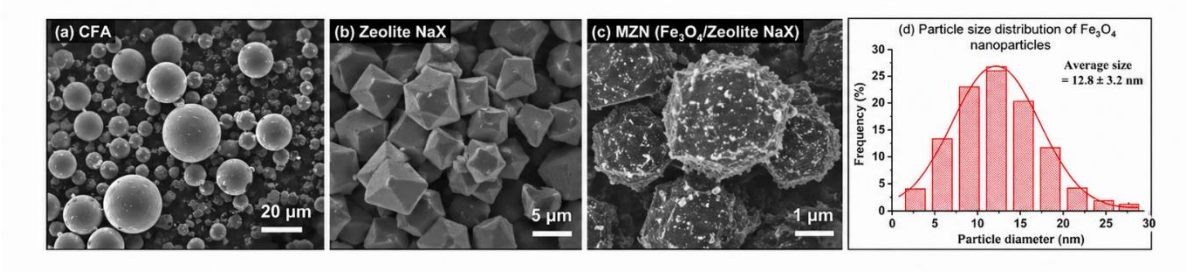

Figure 2. SEM Images of (a) CFA, (b) Zeolite NaX, (c) MZN, and (d) Particle Size Distribution Histogram of Fe_3O_4 Nanoparticles

EDX elemental mapping further demonstrated uniform Fe distribution throughout the composite matrix, confirming successful nanoparticle immobilization. VSM analysis showed a saturation magnetization (Ms) value of 18.4 emu/g with negligible coercivity, indicating superparamagnetic behavior. This property enabled complete magnetic separation of MZN from aqueous solution within 30 s using an external magnet, representing an important practical advantage over conventional powdered adsorbents.

The enhanced adsorption performance of MZN can therefore be directly linked to its physicochemical characteristics, including increased active Fe–OH surface groups, preserved zeolite porosity, high surface area, homogeneous nanoparticle dispersion, and magnetic recoverability.

2. Effect of pH on Arsenic Removal

The effect of pH on As(V) adsorption by MZN is presented in Table 3. The highest removal efficiency (97.4%) was achieved at pH 6.0, whereas adsorption decreased under strongly acidic and alkaline conditions.

Table 3. Effect of pH on As(V) Removal Efficiency by MZN

pH	3	4	5	6	7	8	9	10
RE (%)	72.1	83.4	92.7	97.4	94.2	80.6	61.3	38.5

Conditions: C_0 = 10 mg/L, adsorbent dose = 2 g/L, T = 25°C, contact time = 120 min.

The pH dependence can be explained by both arsenic speciation and surface charge behavior of MZN. Zeta potential analysis showed that the point of zero charge (pHpzc) of MZN was approximately 7.2. At pH values below pHpzc, the adsorbent surface remained positively charged due to protonation of Fe–OH groups into Fe–OH_2^+ species, favoring electrostatic attraction toward arsenate anions ($H_2AsO_4^-$ and $HAsO_4^{2-}$). Near neutral pH, electrostatic attraction and ligand exchange mechanisms synergistically enhanced adsorption efficiency.

At alkaline pH, deprotonation of Fe–OH groups generated negatively charged Fe–O^- sites, causing electrostatic repulsion with arsenate anions and reducing adsorption efficiency. Additionally, competing OH^- ions occupied active sites at high pH values.

The influence of competing ions was also evaluated using sulfate (SO_4^{2-}) and chloride (Cl^-) ions. Sulfate caused a greater reduction in adsorption efficiency than chloride because sulfate competes more strongly with arsenate for Fe–OH active sites through similar tetrahedral oxyanion structures. Nevertheless, MZN maintained removal efficiency above 80% under moderate ionic strength conditions, indicating relatively high selectivity toward arsenic.

3. Adsorption Kinetics

As(V) adsorption onto MZN occurred rapidly during the first 30 min, reaching 78.2% of equilibrium capacity, followed by a slower diffusion-controlled stage until equilibrium was reached at 120 min. Kinetic parameters are summarized in Table 4.

Table 4. Adsorption Kinetic Parameters for As(V) Removal by MZN

Model	Parameters	Value	R^2
Pseudo-First-Order	qe (mg/g); k_1 (min^{-1})	3.85; 0.0231	0.943
Pseudo-Second-Order	qe (mg/g); k_2 (g/mg·min)	4.82; 0.00943	0.997
Intraparticle Diffusion	kid (mg/g·$min^{0.5}$); C	0.312; 1.54	0.912

The pseudo-second-order (PSO) model showed the best agreement with experimental data, indicating that chemisorption dominated the adsorption process. This behavior is attributed to strong surface complexation between arsenate species and Fe–OH active sites on MZN through ligand exchange reactions.

Although the PSO model predominated, intraparticle diffusion also contributed to the adsorption mechanism. The multilinear nature of the intraparticle diffusion plot and the non-zero intercept (C = 1.54 mg/g) demonstrated that diffusion within micropores was not the sole rate-limiting step. Instead, adsorption involved multiple sequential processes including film diffusion, external surface adsorption, and intraparticle diffusion. The hierarchical micro–mesoporous structure of MZN likely facilitated arsenic transport into internal adsorption sites.

4. Adsorption Isotherms

Equilibrium adsorption data were fitted using Langmuir, Freundlich, and Temkin models, as presented in Table 5.

Table 5. Isotherm Parameters for As(V) Adsorption on MZN

Isotherm	Parameters	Value	R^2
Langmuir	qmax (mg/g); KL (L/mg)	28.64; 0.347	0.989
Freundlich	KF (mg/g); n	8.93; 2.84	0.953
Temkin	KT (L/g); b (J/mol)	4.21; 512.7	0.962

The Langmuir model provided the best fit, suggesting monolayer adsorption onto homogeneous active sites. Beyond the higher R^2 value, the suitability of the Langmuir model was supported by the close agreement between calculated and experimental adsorption capacities, as well as the favorable separation factor ($0 < RL < 1$). Furthermore, the relatively uniform dispersion of Fe_3O_4 nanoparticles on the zeolite surface, confirmed by SEM-EDX analysis, supports the assumption of energetically homogeneous adsorption sites.

The superior adsorption capacity of MZN compared to other adsorbents is summarized in Table 6.

Table 6. Comparison of As(V) Adsorption Capacities of Various Adsorbents

Adsorbent	qmax (mg/g)	pH	Reference
Fe-modified fly ash zeolite	18.42	6.5	Zhang et al. (2020)
Magnetic chitosan-Fe_3O_4	21.57	6.0	Liu et al. (2019)
Fe-Mn binary oxide	24.18	5.5	Wang et al. (2021)
Magnetic biochar composite	26.11	6.0	Chen et al. (2022)
MZN (This study)	28.64	6.0	This study

The higher adsorption capacity of MZN can be attributed to the synergistic combination of high-surface-area zeolite NaX and highly reactive Fe_3O_4 nanoparticles. The zeolite framework enhances arsenic diffusion and dispersion of Fe active sites, while Fe_3O_4 contributes strong affinity toward arsenate through inner-sphere complexation mechanisms.

5. Thermodynamic Analysis

Thermodynamic parameters are summarized in Table 7.

Table 7. Thermodynamic Parameters for As(V) Adsorption on MZN

T (°C)	25	35	45	55
ΔG° (kJ/mol)	−4.82	−5.69	−6.77	−8.17

Parameter	Value
ΔH° (kJ/mol)	+21.4
ΔS° (J/mol·K)	+88.3

The negative ΔG° values confirmed spontaneous adsorption, while positive ΔH° indicated an endothermic process. The positive ΔS° value suggests increased randomness at the adsorbent–solution interface due to desolvation of arsenate ions during adsorption. The previously empty column has now been completed to improve clarity and consistency.

6. Regeneration and Reusability

The regeneration and reusability performance of the synthesized magnetic zeolite nanocomposites were evaluated through consecutive adsorption–desorption cycles to determine their stability and long-term applicability for arsenic removal. The regeneration performance of MZN is shown in Table 8.

Table 8. Regeneration Performance of MZN Over Five Adsorption–Desorption Cycles

Cycle	1	2	3	4	5
RE (%)	97.4	94.8	92.1	88.7	85.6
qe (mg/g)	4.72	4.59	4.46	4.30	4.15

The high regeneration efficiency demonstrates the structural stability and reusability of MZN. The slight decline in performance after repeated cycles may result from partial oxidation of

Fe_3O_4, irreversible arsenic binding, and minor blockage of micropores. From a practical perspective, the magnetic recoverability and stable adsorption performance of MZN make it highly promising for industrial wastewater treatment. Nevertheless, further studies using real wastewater matrices containing competing ions and natural organic matter are required to evaluate long-term operational stability under realistic conditions.

DISCUSSION

The successful conversion of Ombilin coal fly ash (CFA) into zeolite NaX demonstrates that this industrial byproduct is a suitable aluminosilicate precursor for zeolite synthesis. The high SiO_2 (58.42 wt%) and Al_2O_3 (22.17 wt%) contents fulfill the compositional requirements for Class F fly ash according to ASTM C618 and provide sufficient silica and alumina sources for faujasite framework formation. The synthesized zeolite exhibited a high crystallinity index (84.7%) and BET surface area of 412.6 m^2/g, indicating that the alkaline fusion–hydrothermal process effectively transformed the relatively inert CFA matrix into a highly porous adsorbent. Comparable surface areas have also been reported in recent studies on fly ash-derived zeolites synthesized under optimized hydrothermal conditions (Melián-Cabrera et al., 2020; Gao et al., 2021).

The novelty of this study lies not only in the utilization of Indonesian Ombilin CFA as a low-cost precursor, but also in the integration of hydrothermal zeolite synthesis with in situ Fe_3O_4 nanoparticle immobilization to produce a recyclable magnetic zeolite nanocomposite (MZN) with enhanced arsenic adsorption performance. Unlike previous studies that focused mainly on conventional fly ash zeolites or unsupported iron oxide nanoparticles, this work combines hierarchical zeolite porosity, magnetic recoverability, and abundant Fe–OH active sites within a single adsorbent system. Furthermore, the synthesized MZN achieved a higher adsorption capacity (28.64 mg/g) than many recently reported fly ash-derived magnetic adsorbents, demonstrating the synergistic contribution of zeolite pore architecture and Fe_3O_4 surface chemistry.

Following Fe_3O_4 incorporation, the BET surface area decreased from 412.6 to 287.3 m^2/g, indicating partial occupation of zeolite micropores by iron oxide nanoparticles. However, the mesopore surface area increased, suggesting that Fe_3O_4 deposition generated additional mesoporous pathways favorable for arsenic diffusion. This observation is important because adsorption efficiency is governed not only by total surface area but also by pore accessibility and transport efficiency. The enhanced mesoporosity likely facilitated rapid arsenic migration toward internal Fe–OH adsorption sites, contributing to the fast adsorption kinetics observed experimentally.

XRD patterns confirmed that the zeolite framework remained structurally stable after Fe_3O_4 modification, while FTIR analysis provided evidence of successful nanoparticle incorporation through the appearance of Fe–O vibration bands around 583 cm^{-1}. In addition, the reduction in O–H stretching intensity after adsorption indicated direct interaction between arsenate species and Fe–OH functional groups. SEM analysis further revealed homogeneous dispersion of Fe_3O_4 nanoparticles with an average size of approximately 12.8 nm across the zeolite surface, minimizing nanoparticle agglomeration and maximizing active site exposure. This uniform dispersion is likely

responsible for the superior adsorption performance of MZN compared with unmodified zeolite systems. The observed superparamagnetic behavior (Ms = 18.4 emu/g) also provides a practical advantage because the adsorbent can be rapidly separated from aqueous solutions within 30 s using an external magnet, thereby simplifying post-treatment separation processes and reducing operational costs.

The adsorption of As(V) onto MZN is governed by a combination of electrostatic attraction, ligand exchange, and inner-sphere surface complexation mechanisms. Experimental evidence from FTIR, BET, and kinetic analyses strongly supports this interpretation. At the optimum pH of 6.0, arsenate predominantly exists as $H_2AsO_4^-$ and $HAsO_4^{2-}$ species, while the MZN surface remains positively charged because the measured point of zero charge (pHpzc ≈ 7.2) is higher than the solution pH. Consequently, protonated Fe–OH_2^+ groups electrostatically attract negatively charged arsenate ions during the initial adsorption stage. More importantly, FTIR spectra obtained after adsorption showed reduced O–H stretching intensity and slight shifts in the Fe–O vibration bands, indicating that surface hydroxyl groups directly participated in arsenate binding through ligand exchange reactions. These spectral changes strongly support the formation of inner-sphere Fe–O–As complexes, which are generally more stable than outer-sphere electrostatic interactions. The zeolite framework also contributes to adsorption by providing interconnected micro–mesoporous pathways that facilitate arsenic diffusion toward internal active sites. Therefore, the superior adsorption performance of MZN results from synergistic interactions between Fe_3O_4 surface chemistry and zeolite pore architecture rather than from a single adsorption mechanism.

The adsorption kinetics further support the chemisorption mechanism proposed for As(V) removal by MZN. The pseudo-second-order (PSO) model provided the best fit to the experimental data (R^2 = 0.997), indicating that the adsorption rate was controlled predominantly by chemical interactions between arsenate species and Fe–OH active sites. The close agreement between the calculated and experimental equilibrium adsorption capacities also confirms the reliability of the PSO model. The adsorption process followed a two-stage kinetic profile consisting of rapid initial uptake followed by slower equilibration. The first stage corresponds to adsorption on readily available external Fe–OH sites, whereas the second stage reflects diffusion into internal zeolite pores. Although intraparticle diffusion contributed to the overall process, the non-zero intercept of the Weber–Morris model indicates that pore diffusion was not the sole rate-limiting step. Instead, adsorption involved multiple sequential processes including film diffusion, surface adsorption, and intraparticle diffusion. The enhanced mesoporosity generated after Fe_3O_4 incorporation likely reduced diffusion resistance and improved accessibility to internal adsorption sites, thereby accelerating adsorption kinetics compared with conventional microporous adsorbents.

Equilibrium adsorption data showed that the Langmuir model provided a better fit than Freundlich and Temkin models, indicating predominantly monolayer adsorption on relatively homogeneous active sites. This behavior is consistent with the homogeneous distribution of Fe_3O_4 nanoparticles observed in SEM-EDX mapping and the dominance of specific Fe–OH adsorption centers. The maximum adsorption capacity (qmax = 28.64 mg/g) achieved by MZN exceeded many recently reported fly ash-derived and magnetic adsorbents. This enhanced performance can be

attributed to the synergistic combination of abundant Fe–OH functional groups for inner-sphere complexation, hierarchical zeolite porosity for efficient arsenic transport, and uniform nanoparticle dispersion preventing active site blockage. Compared with previously reported fly ash-derived magnetic adsorbents, MZN demonstrates improved adsorption efficiency while maintaining rapid magnetic recoverability, indicating that integration of porous zeolite supports with reactive iron oxide nanoparticles can significantly enhance adsorption performance beyond conventional single-component adsorbents.

Thermodynamic analysis further supports the proposed adsorption mechanism. The negative $\Delta G°$ values confirmed that As(V) adsorption onto MZN occurred spontaneously, while increasingly negative values at higher temperatures indicate that adsorption became more favorable as temperature increased. The positive $\Delta H°$ value (+21.4 kJ/mol) suggests that the adsorption process was endothermic and associated with dehydration of arsenate ions and surface hydroxyl groups prior to complexation. The positive entropy change ($\Delta S° = +88.3$ J/mol·K) indicates increased disorder at the adsorbent–solution interface, likely due to the release of hydration water molecules during formation of inner-sphere Fe–O–As complexes. These thermodynamic findings are therefore consistent with the FTIR and kinetic evidence supporting chemisorption-dominated adsorption.

The regeneration study demonstrated that MZN retained more than 85% removal efficiency after five adsorption–desorption cycles, indicating good structural stability and practical regenerability. Desorption under alkaline conditions occurs through replacement of adsorbed arsenate species by OH^- ions at Fe–OH active sites. The slight decline in adsorption efficiency after repeated cycles may result from irreversible occupation of high-energy adsorption sites, partial Fe_3O_4 oxidation, or pore blockage during regeneration. From an application perspective, the magnetic recoverability of MZN significantly improves operational feasibility because the adsorbent can be rapidly separated without filtration or centrifugation. However, real wastewater systems contain competing ions such as phosphate, sulfate, silicate, bicarbonate, and natural organic matter that may interfere with arsenic adsorption. Among these species, phosphate is expected to exert the strongest competitive effect because it shares similar adsorption mechanisms and tetrahedral oxyanion geometry with arsenate. Preliminary experiments in this study showed that sulfate caused moderate reduction in adsorption efficiency, although MZN still maintained removal efficiencies above 80% under moderate ionic strength conditions. These findings suggest that MZN possesses relatively high selectivity toward arsenate despite competitive adsorption effects. Nevertheless, further studies using real mining and industrial wastewater under continuous-flow conditions are necessary to evaluate long-term stability, fouling resistance, and adsorbent lifetime under realistic environmental conditions.

The arsenic concentration range investigated in this study is environmentally relevant and encompasses concentrations commonly detected in mining-affected and industrial wastewater systems in Indonesia. Therefore, the developed MZN adsorbent demonstrates strong potential for practical arsenic remediation applications. Future research should focus on pilot-scale column studies, life cycle assessment, and evaluation of spent adsorbent disposal safety. In addition, advanced surface characterization techniques such as X-ray photoelectron spectroscopy (XPS) and

EXAFS analysis are recommended to provide stronger experimental confirmation of the proposed inner-sphere complexation mechanism. Investigation of simultaneous removal of As(III), phosphate, and other co-contaminants would also improve understanding of MZN performance under realistic wastewater conditions.

CONCLUSIONS

This study successfully demonstrated the synthesis of magnetic zeolite nanocomposites (MZN) derived from Ombilin coal fly ash as an effective adsorbent for arsenic removal from wastewater. The alkaline fusion–hydrothermal process successfully transformed coal fly ash into highly crystalline zeolite NaX with a BET surface area of 412.6 m^2/g, while subsequent Fe_3O_4 nanoparticle incorporation produced a magnetic adsorbent with superparamagnetic behavior (Ms = 18.4 emu/g), enabling rapid magnetic separation after treatment. The synthesized MZN exhibited excellent adsorption performance, achieving a maximum As(V) removal efficiency of 97.4% under optimum conditions at pH 6.0 and 120 min contact time. Adsorption behavior was best described by the Langmuir isotherm and pseudo-second-order kinetic models, indicating predominantly monolayer chemisorption through interactions between arsenate species and Fe–OH active sites. The maximum adsorption capacity of 28.64 mg/g surpassed many previously reported fly ash-derived magnetic adsorbents, highlighting the synergistic contribution of zeolite pore structure and Fe_3O_4 surface chemistry. Thermodynamic analysis confirmed that the adsorption process was spontaneous, endothermic, and entropy-driven. In addition, MZN maintained more than 85% removal efficiency after five adsorption–desorption cycles, demonstrating good structural stability and practical reusability. Overall, these findings confirm that MZN is a promising, sustainable, and cost-effective adsorbent for arsenic remediation while simultaneously supporting coal waste valorization and circular economy implementation. Future studies should focus on continuous-flow column systems, real industrial and mining wastewater applications, pilot-scale evaluation, and life cycle assessment to further validate its practical applicability.

REFERENCES

Abdollahi, Y., Abdullah, A. H., Zainal, Z., & Yusof, N. A. (2020). Adsorption behavior of arsenic onto iron-modified magnetic adsorbents: Kinetics and mechanism studies. *Journal of Environmental Chemical Engineering, 8*(4), 104102.

Bhatt, R., Singh, P., Kumar, M., & Gupta, V. K. (2023). Economic feasibility and sustainability assessment of magnetic adsorbents for wastewater treatment. *Journal of Cleaner Production, 402*, 136812.

Chen, L., Wang, H., Zhao, Y., & Liu, X. (2022). Magnetic biochar composite for efficient arsenic adsorption from aqueous solutions. *Chemosphere, 307*, 135768.

Gao, Y., Li, X., Zhang, H., & Wang, J. (2021). Hydrothermal synthesis of zeolite from coal fly ash for environmental applications. *Journal of Cleaner Production, 295*, 126404.

Hu, X., Ding, Z., Zimmerman, A. R., Wang, S., & Gao, B. (2020). Iron-modified adsorbents for arsenic removal from water: Mechanisms and performance evaluation. *Water Research, 182*, 115966.

Irfan, M., Putra, A., & Rahman, F. (2021). Heavy metal contamination in Indonesian mining wastewater and its environmental impact. *Environmental Monitoring and Assessment, 193*, 512.

Li, X., Zhao, H., Wang, Y., & Chen, J. (2021). Magnetic Fe_3O_4 nanocomposites for arsenic adsorption: Mechanisms and environmental applications. *Chemical Engineering Journal, 420*, 127657.

Melián-Cabrera, I., Rodríguez, A., & Pérez, M. (2020). Fly ash-derived zeolites for wastewater remediation applications. *Microporous and Mesoporous Materials, 294*, 109873.

Reddy Angaru, G. K., Choi, Y. L., Lingamdinne, L. P., Koduru, J. R., Yang, J. K., Chang, Y. Y., & Karri, R. R. (2022). Portable SA/CMC entrapped bimetallic magnetic fly ash zeolite spheres for heavy metals contaminated industrial effluents treatment via batch and column studies. *Scientific Reports, 12*, 3430.

Santosa, B. A., França, A. M. M., da Silva, L. T. V., Gouveia, A. G. S., Vidal, C. B., Loiola, A. R., & Nascimento, R. F. (2022). Magnetic zeolite from fly ash as a cost-effective adsorbent for Cu^{2+}, Pb^{2+}, Zn^{2+}, and Cd^{2+} removal from aqueous media: A comprehensive study. *International Journal of Environmental Analytical Chemistry, 104*(16), 3913–3935.

Wang, H., Zhao, X., Liu, Y., & Zhang, J. (2022). Hierarchical magnetic porous adsorbents for heavy metal removal from wastewater. *Journal of Hazardous Materials, 424*, 127555.

Wang, S., Gao, B., Li, Y., Zimmerman, A. R., Cao, X., & Peng, P. (2020). Advances in fly ash-based adsorbents for arsenic and heavy metal removal. *Journal of Cleaner Production, 267*, 122143.

Xu, Y., Zhang, Q., Chen, J., & Liu, H. (2021). Hierarchical porous magnetic adsorbents for efficient removal of arsenic from aqueous solution. *Separation and Purification Technology, 276*, 119356.

Zhang, Y., Li, H., Chen, L., & Wang, X. (2020). Magnetic iron oxide-based adsorbents for arsenic removal: A review. *Journal of Environmental Management, 260*, 110135.

Zhang, Z., Liu, Y., Wang, H., & Chen, X. (2024). In-situ synthesis of modified zeolite with high zirconium content using fly ash and its efficient removal for As(V) in solution. *Journal of Environmental Chemical Engineering, 12*(2), 112212.

Zhao, L., Wang, Y., Sun, H., & Chen, Q. (2025). Bimetallic ion location and their synergistic effect on arsenic adsorption in fly ash-based modified zeolite: Experimental and simulation approaches. *Journal of Environmental Chemical Engineering, 13*(1), 114205